Extended Data Figures and tables

Dinuclear titanium on TS-1 for propylene epoxidation at alkaline condition

Kwang Hyun Kim[1,2,†], Taehyeon Kim[1,†], Haneul Kim[1,2], June Sung Lim[1], Myohwa Ko[1], Wonjoo Jin[1], Kwanyong Seo[1,3], Sang Hoon Joo[4], Sung June Cho[5*], Ji-Wook Jang[1,3*], Ja Hun Kwak[1,2*]

[1] School of Energy and Chemical Engineering, Ulsan National Institute of Science and Technology (UNIST), 50 UNIST-gil, Ulsan 44919, Republic of Korea

[2] Center for Multidimensional Carbon Materials (CMCM), Institute for Basic Science (IBS), 50 UNIST-gil, Ulsan 44919, Republic of Korea

[3]Graduate School of Carbon Neutrality, Ulsan National Institute of Science and Technology (UNIST), Ulsan 44919, Republic of Korea.

[4]Department of Chemistry, Seoul National University, Seoul 08826, Republic of Korea

[5] Department of Chemical Engineering, Chonnam National University, 77 Yongbong-Ro, Buk-Gu, Gwangju, 61186, Republic of Korea

[†]These authors contributed equally.

[*]Corresponding author: jhkwak@unist.ac.kr (JHK), jwjang@unist.ac.kr (JWJ), sjcho@chonnam.ac.kr (SJC)

Contents

List of tables

List of figures

with and without the gas-diffusion electrode.

Extended Data Fig. 13 | PO production in electro-heterogeneous catalytic system at 0.5 V vs. RHE.

Extended Data Fig. 14 | Solar to hydrogen peroxide conversion efficiency difference compared with previous work.

Extended Data Fig. 15 | Scanning electron microscopy images of different catalysts. a, TS-1(100); b, TS-1(100)-m; c, TS-1(33); d, TS-1(33)-m.

Extended Data Fig. 16 | Transmission electron microscopy images of TS-1(33) (left) and TS-1(33)-m (right).

Extended Data Fig. 17 | N_2 adsorption (●)/desorption (○) isotherms of TS-1 and modified TS-1.

Extended Data Fig. 18 | Fourier transform infrared spectra of different catalysts. a, TS-1 and modified TS-1. b, Magnifications of a in the range of 3000 to 3800 cm^{-1}.

Extended data Tables

	Propylene glycol production (μmol)		
	DI water	0.1 M NaPi at pH 6	0.1 M NaPi at pH 11
TS-1(100)	1	0	0
TS-1(100)-m	28	0	0
TS-1(33)	39	0	0
TS-1(33)-m	120	0	0

Extended Data Table 1 | Propylene glycol production over TS-1 samples after 6 h of propylene epoxidation in deionized water and 0.1 M sodium phosphate (NaPi) aqueous solution with pH 6 and 11.

Wavenumber (cm^{-1})	Interpretation	Reference
520	TiO_2 anatase	[1]
638	TiO_2 anatase	[1]
970	the asymmetric stretching of the TiO_4 unit	[1,2]

Extended Data Table 2 | Raman peak assignments.

Pair	CN	R (Å)	ΔE (eV)	R (%)
Ti-O	4	1.82 ± 0.01		
Ti-O	-	-	-11.7 ± 4.2	5.2
Ti-O	-	-		
Ti-Ti	1	2.97 ± 0.03		

Extended Data Table 3 | Structural parameters for TS-1(33) extracted from its fitted Ti K-edge EXAFS spectrum recorded under ambient conditions.

Pair	CN	R (Å)	ΔE (eV)	R (%)
Ti-O (Green)	2	1.86 ± 0.03		
Ti-O (Blue)	2	2.05 ± 0.12	0.4 ± 7.7	1.15
Ti-O (Red)	1	2.36 ± 0.03		
Ti-Ti	1	3.12 ± 0.09		

Extended Data Table 4 | Structural parameters of TS-1(33)-m extracted from its fitted Ti K-edge EXAFS spectrum recorded under ambient conditions.

Sample name	Ti structure	Na presence	E_a for Forward reaction (eV)	*E*a for Backward reaction (eV)
MFI-1Ti-H	*mononuclear*	no	0.0000	3.0532
MFI-1Ti-Na	*mononuclear*	yes	0.4008	2.8551
MFI-2Ti-H	*dinuclear*	no	0.0916	2.5891
MFI-2Ti-Na	*dinuclear*	yes	0.0405	2.8041

Extended Data Table 5 | Summary of the CI-NEB simulation for the propylene to PO conversion in the zeolite cavity containing catalytically active Ti sites.

	Si/Ti[a]	BET area (m^2 g^{-1})	Pore volume (cm^3 g^{-1})[b]
TS-1(100)	100	483	0.45
TS-1(100)-m	100	422	0.47
TS-1(33)	33	504	0.51
TS-1(33)-m	33	449	0.51

[a] molar ratio of synthesis gel. [b] Estimated from the adsorption isotherm at a relative pressure of ~ 0.99.

Extended Data Table 6 | Properties of TS-1(100), TS-1(100)-m, TS-1(33), and TS-1(33)-m.

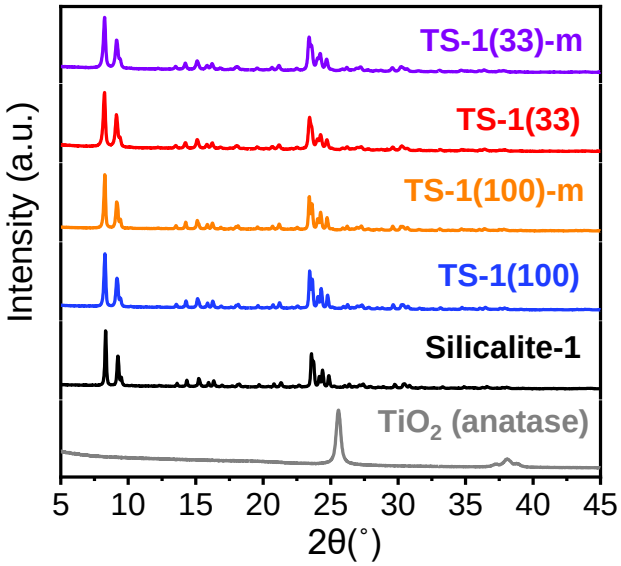

Extended Data Fig. 1 | X-ray diffraction patterns of TiO_2 (anatase), silicalite-1, TS-1 and modified TS-1.

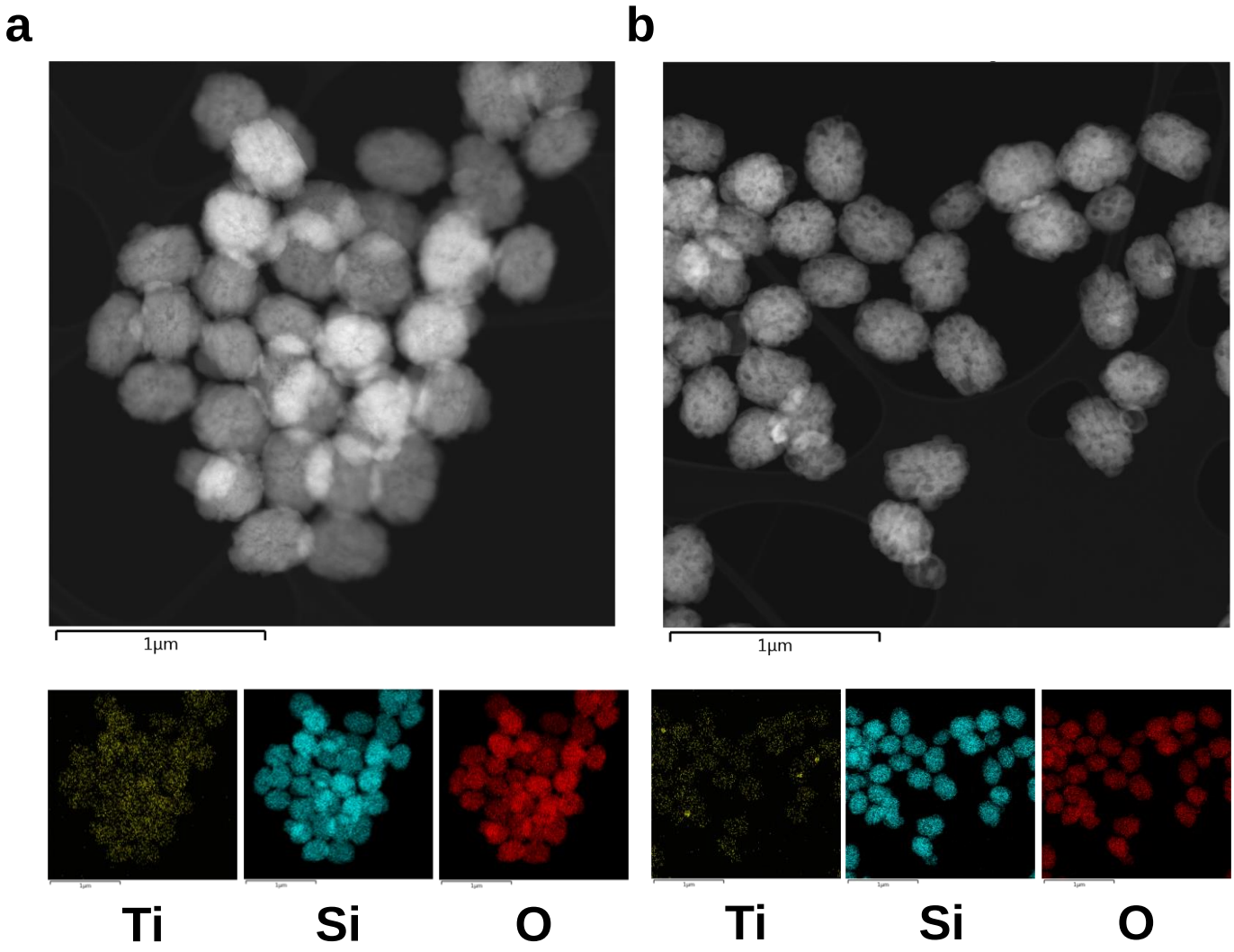

Extended Data Fig. 2 | Scanning transmission electron microscopy–energy-dispersive X-ray spectroscopy images of different catalysts. a, TS-1(33) and **b,** TS-1(33)-m.

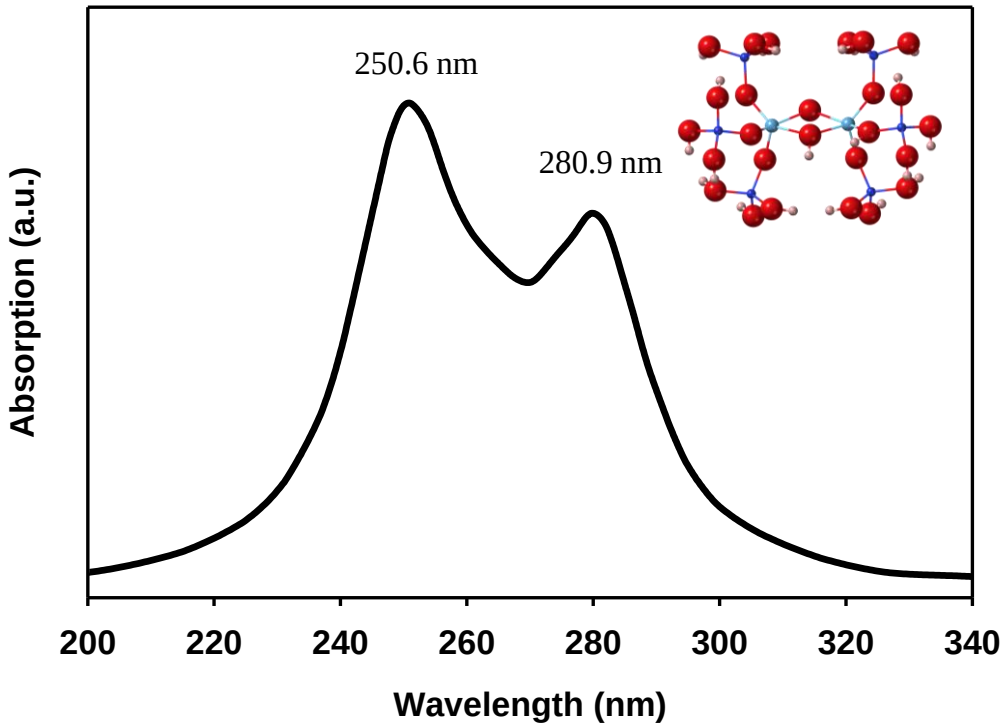

Extended Data Fig. 3 | UV-vis spectrum of the dinuclear complex simulated using the GAMESS package with CIS/6-31G.

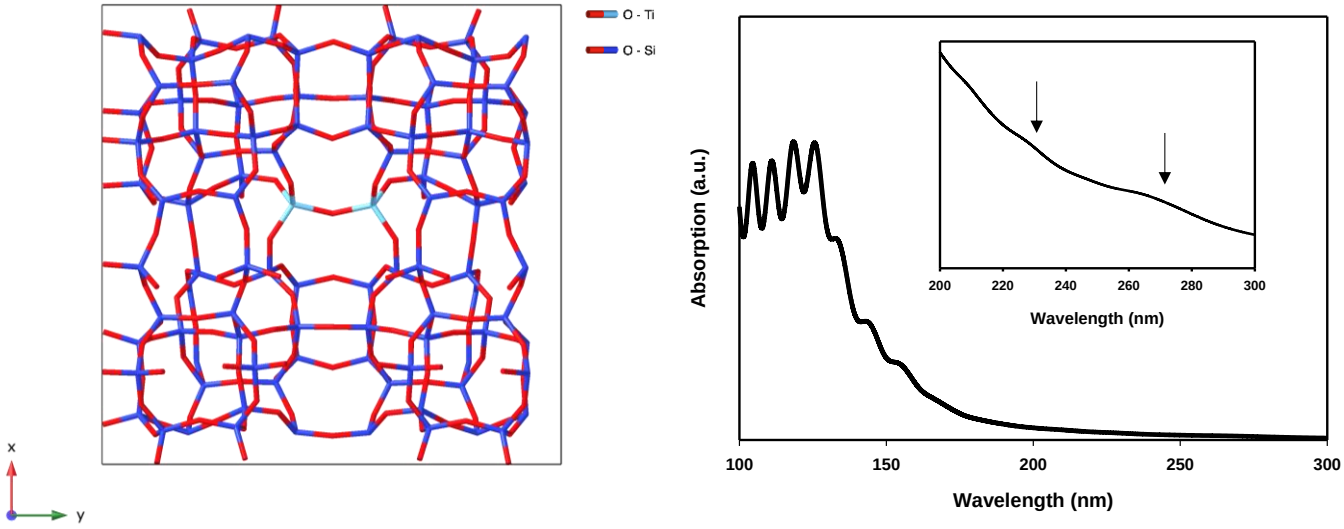

Extended Data Fig. 4 | UV-vis spectrum of the dinuclear complex simulated through Time-Dependent Density Functional Theory (TDDFT) calculations using the ultrasoft pseudopotential implemented in the Quantum Espresso package.

Using the Quantum Espresso package, we optimized the zeolite containing Ti at various T-sites, employing a norm-conserving ultrasoft pseudopotential of 52 Ry and a cutoff of 575 Ry for the wavefunction and charge while only considering the Γ-point. The most stable zeolite incorporating Ti within its framework was used to construct the TS-1 model, which featured dinuclear Ti species.

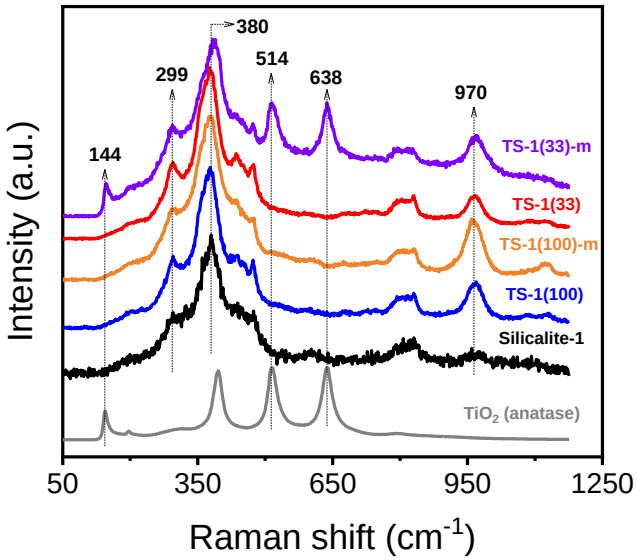

Extended Data Fig. 5 | Raman spectra of TiO_2 (anatase), silicalite-1, TS-1, and modified TS-1 measured using excitation at 532 nm.

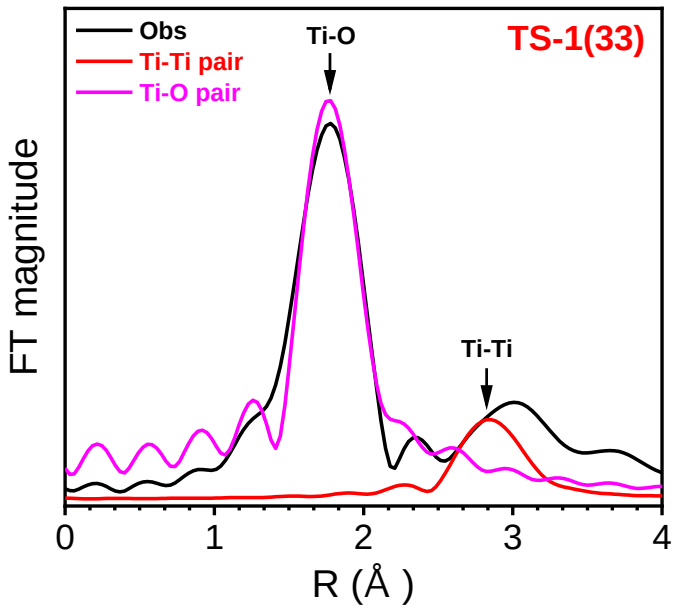

Extended Data Fig. 6 | Fourier Transform (FT) magnitude of Ti K-edge extended X-ray absorption fine structure (EXAFS) signal for TS-1(33).

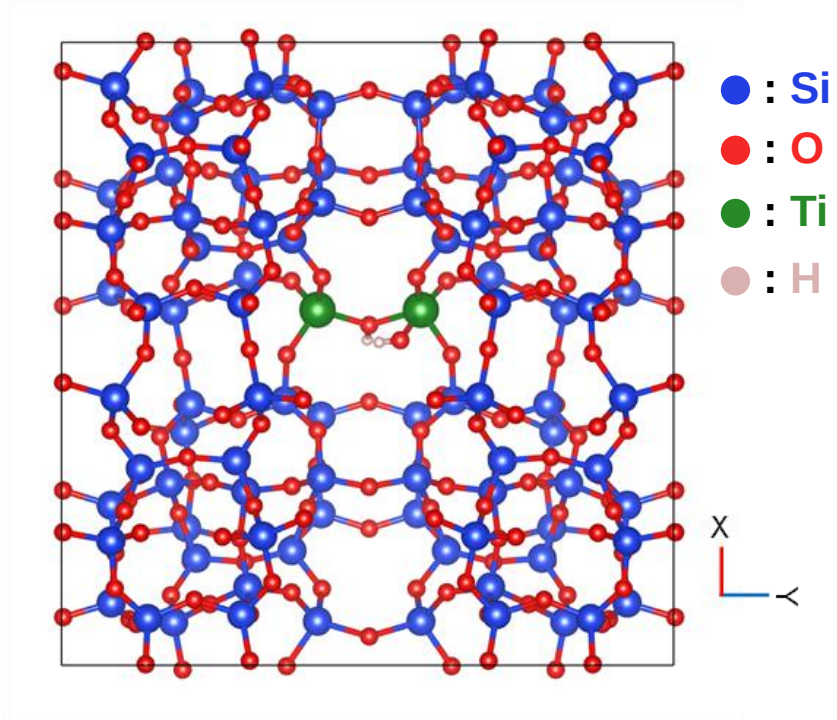

Extended Data Fig. 7 | Visual representation of the geometry optimization calculation for the dinuclear complex using the ultrasoft pseudopotential of the Quantum Espresso package. As optimization progressed, bridging oxygen was formed and subsequently stabilized.

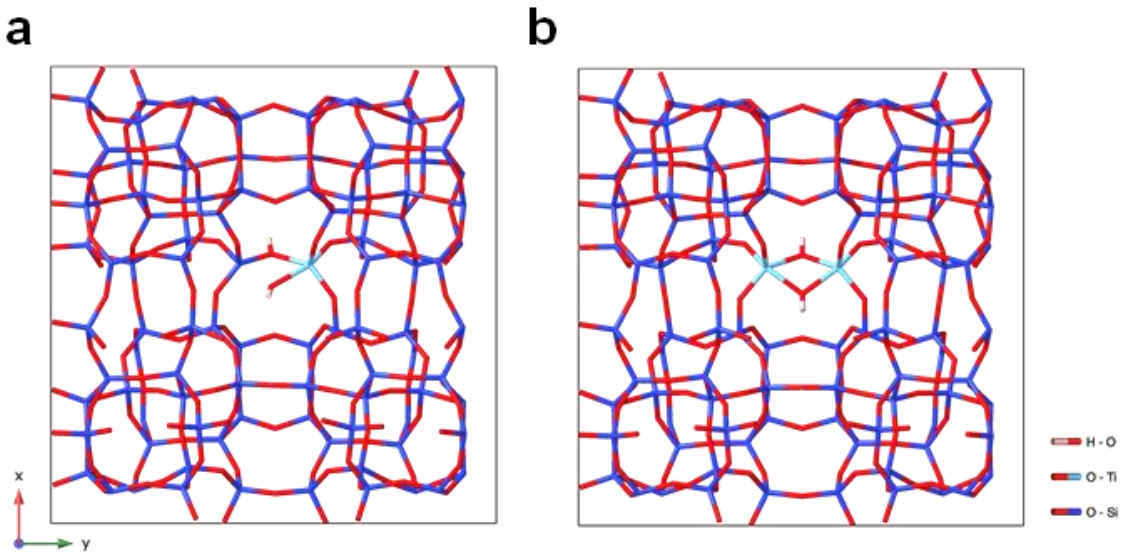

Extended Data Fig. 8 | Optimized structures of different Ti sites. Structures of **a,** mononuclear and **b,** dinuclear Ti sites in TS-1 calculated using the ultrasoft pseudopotential of the *Quantum Espresso* package.

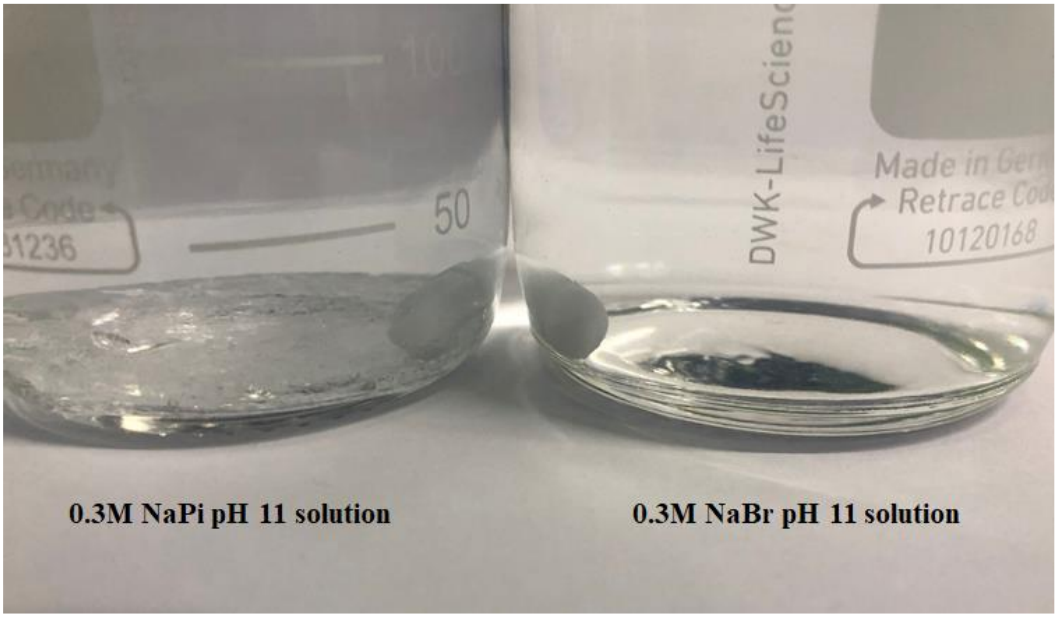

Extended Data Fig. 9 | Salt generation issue in NaPi solution.

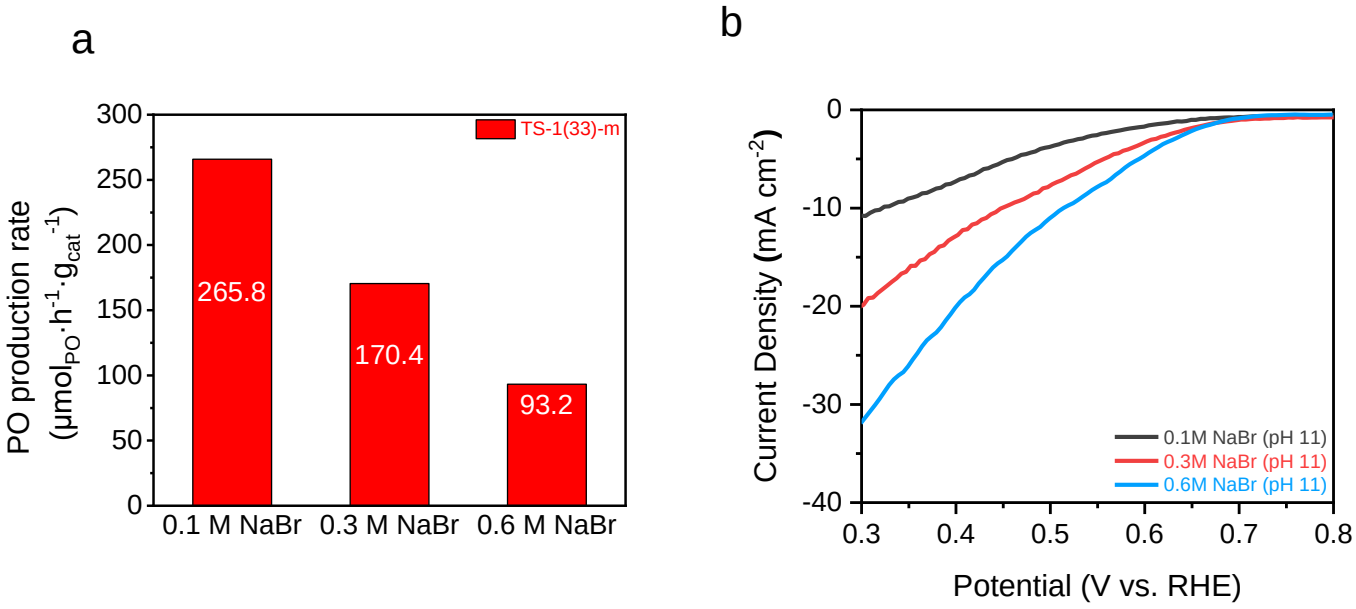

Extended Data Fig. 10 | Optimization of NaBr concentration for the operation of TS-1(33)-m and graphitic ordered mesoporous carbon (GOMC). a, PO production rate of TS-1 (33)-m at different NaBr concentrations. **b,** *I*–*V* curves of GOMC recorded at different NaBr concentrations.

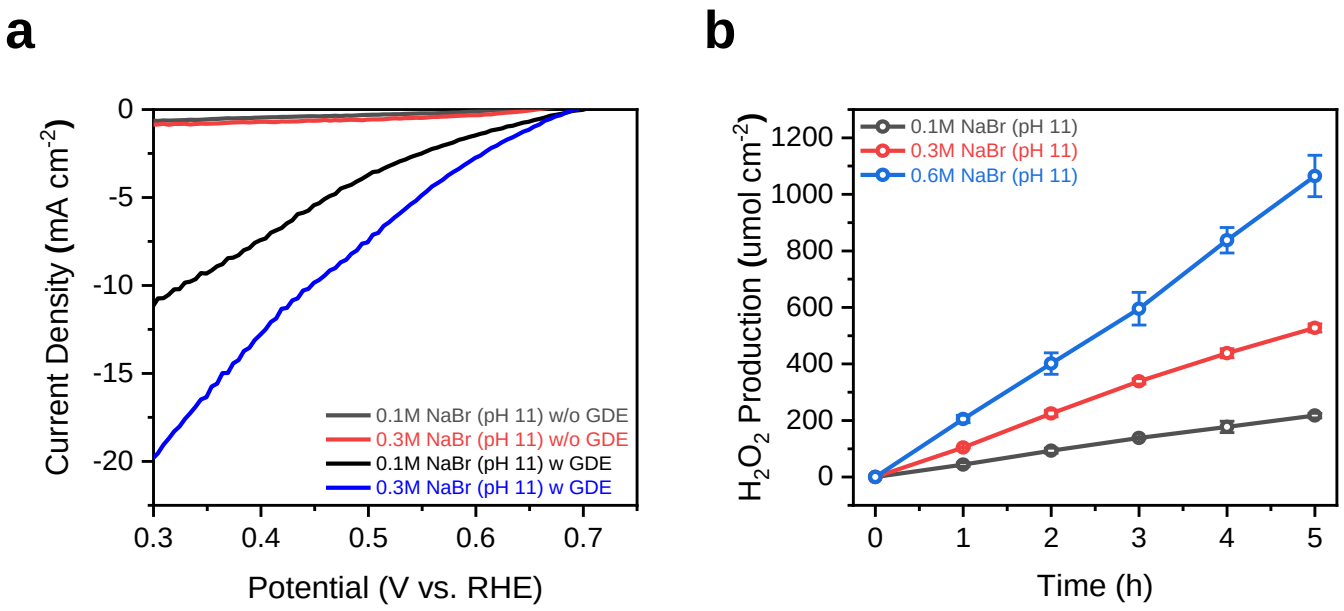

Extended Data Fig. 11 | Performance of electrocatalyst at various concentration conditions a, *I–V* curves of GOMC recorded under various solution conditions with and without the gas-diffusion electrode. **b,** H_2O_2 production at pH 11, 0.5 V vs. the reversible hydrogen electrode (RHE), and different NaBr concentrations.

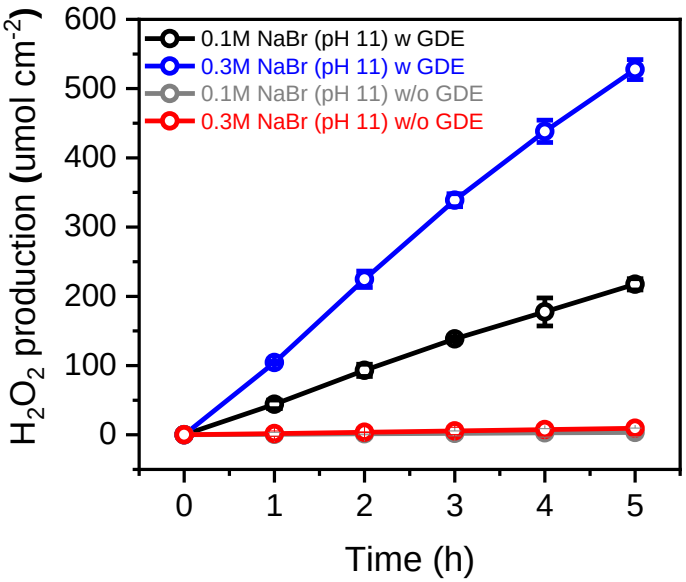

Extended Data Fig. 12 | H_2O_2 production over GOMC at 0.5 V vs. RHE in solutions with and without the gas-diffusion electrode.

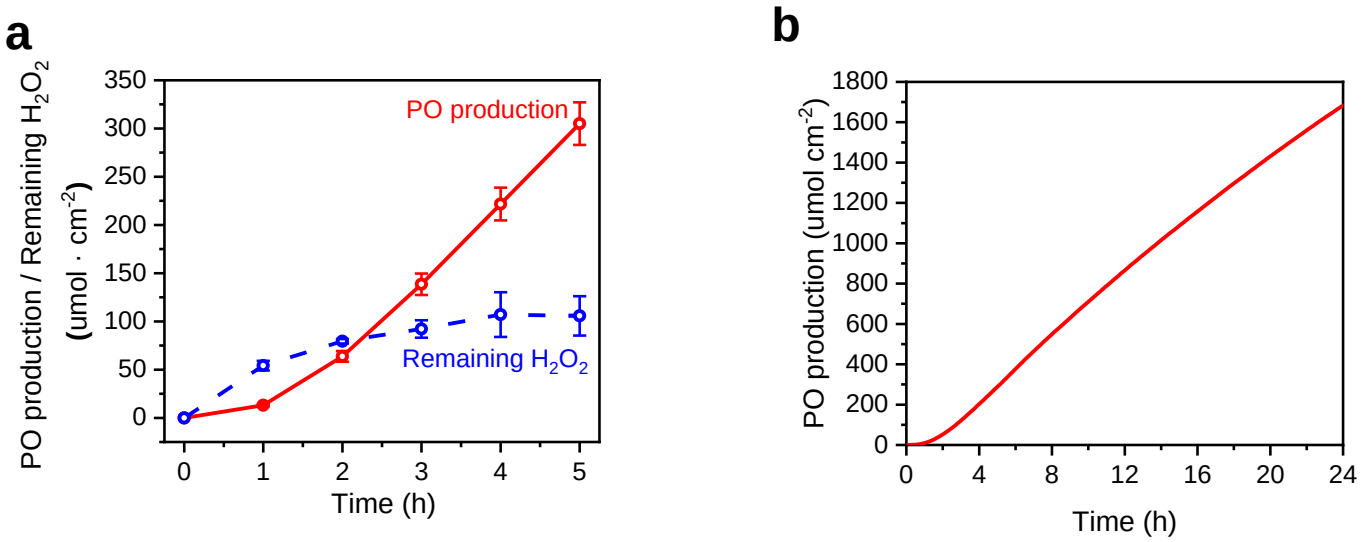

Extended Data Fig. 13 | PO production in electro-heterogeneous catalytic system at 0.5 V vs. RHE.

a, PO production and remaining H_2O_2 for 5 h reaction**. b,** PO production for 24 h reaction.

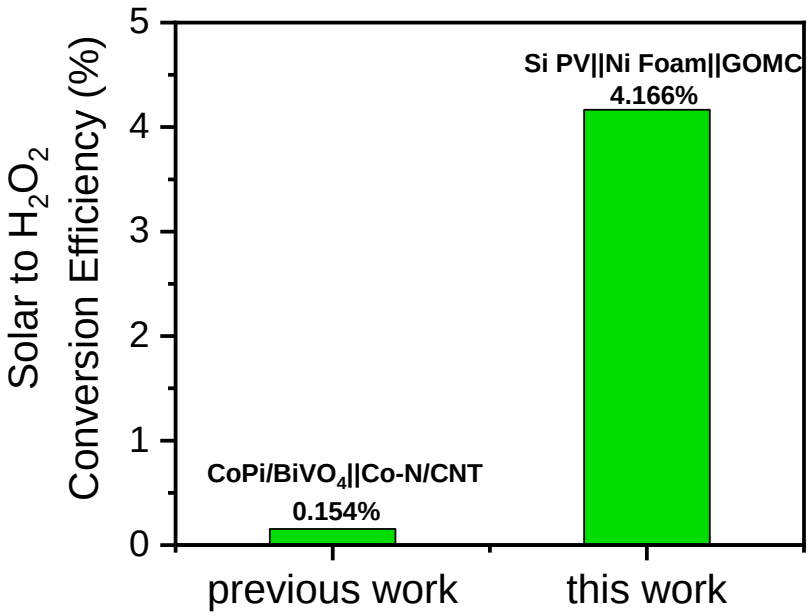

Extended Data Fig. 14 | Solar to hydrogen peroxide conversion efficiency difference compared with previous work[5].

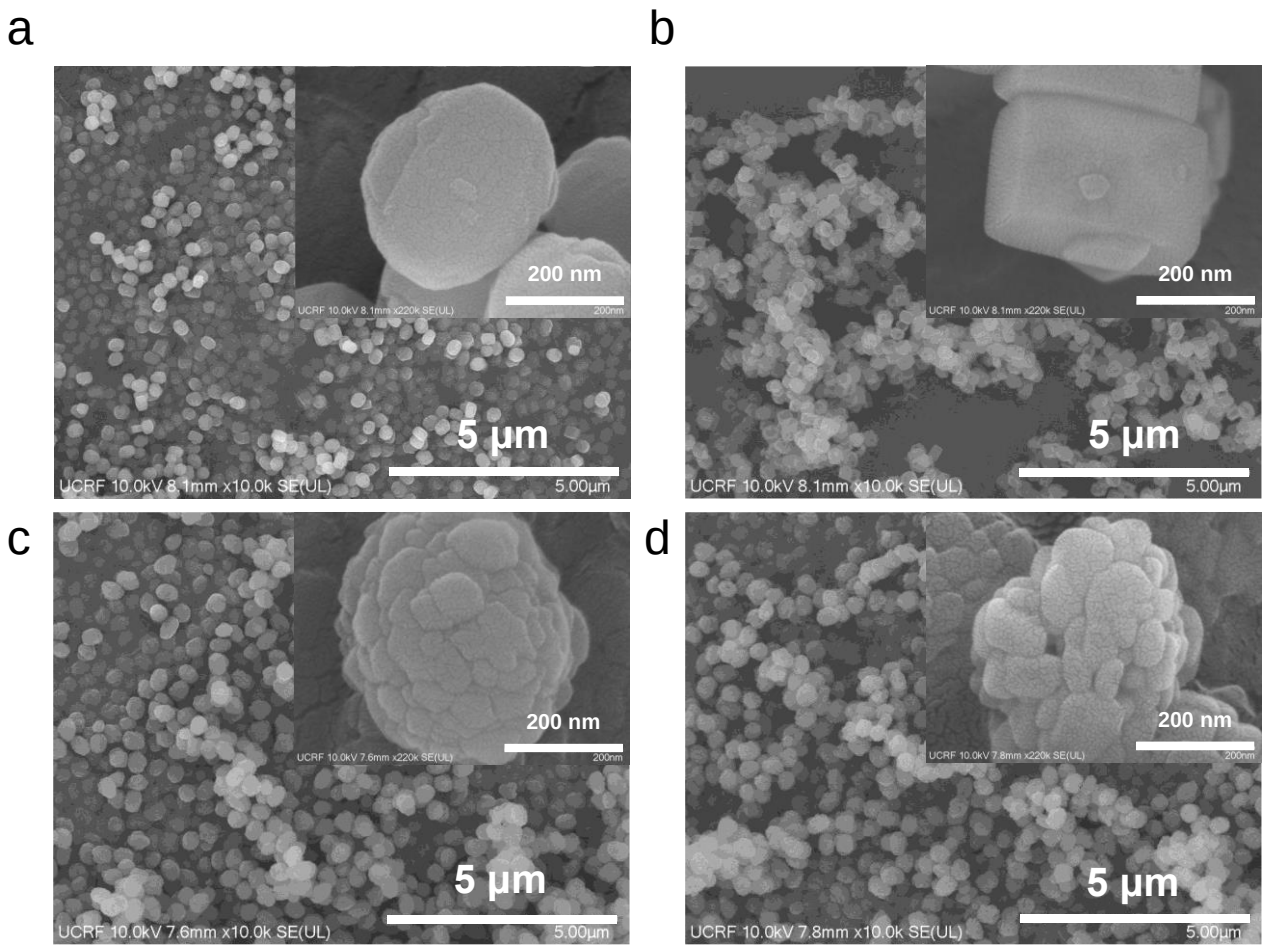

Extended Data Fig. 15 | Scanning electron microscopy images of different catalysts. a, TS-1(100); **b,** TS-1(100)-m; **c,** TS-1(33); **d,** TS-1(33)-m.

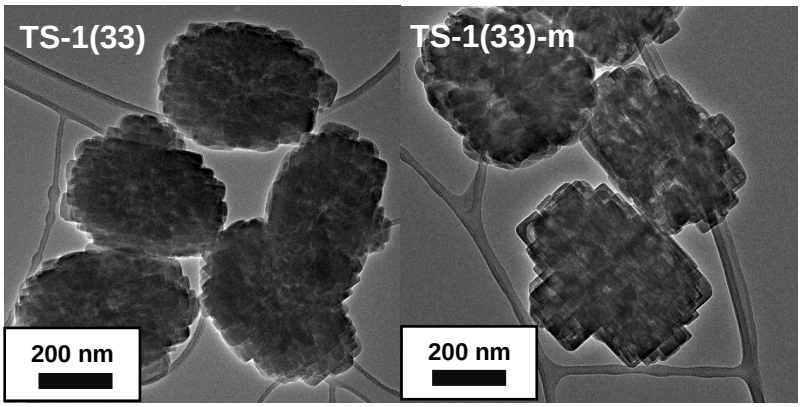

Extended Data Fig. 16 | Transmission electron microscopy images of TS-1(33) (left) and TS-1(33)-m (right).

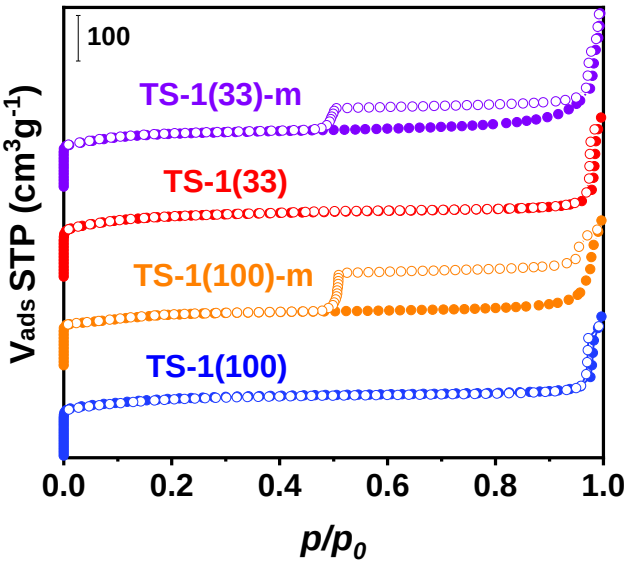

Extended Data Fig. 17 | N_2 adsorption (●)/desorption (○) isotherms of TS-1 and modified TS-1.

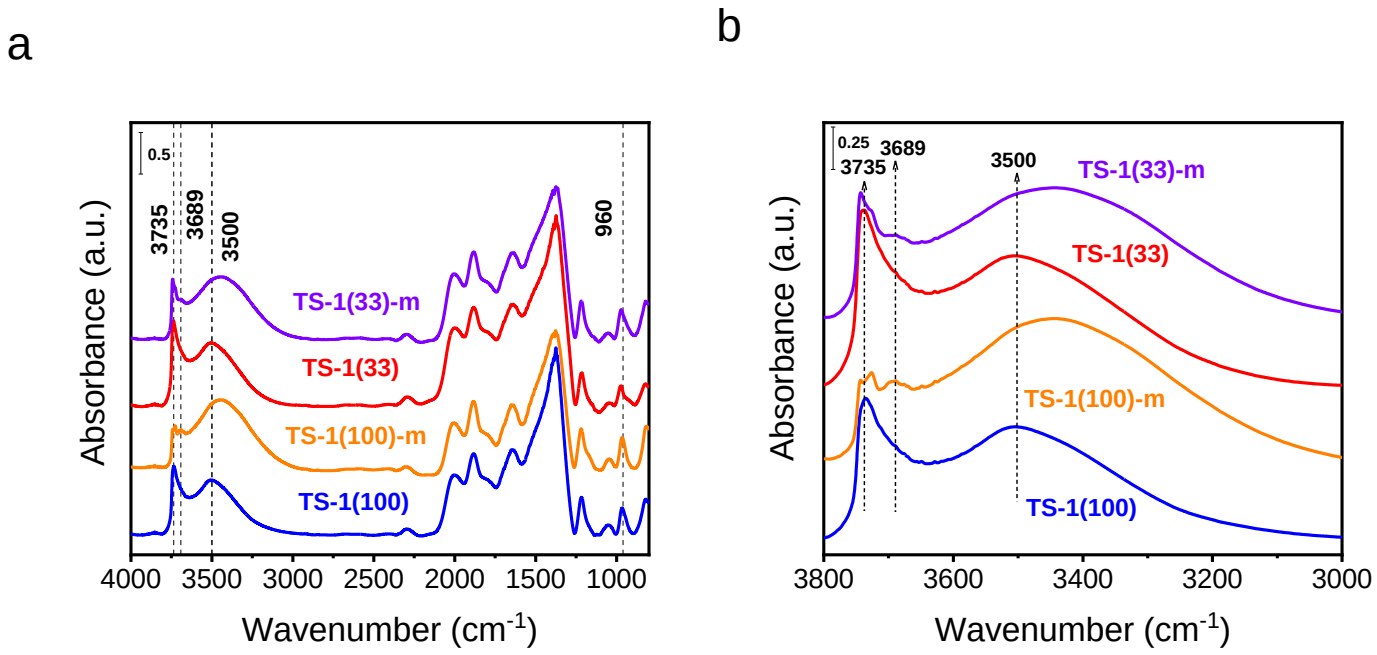

Extended Data Fig. 18 | Fourier transform infrared spectra of different catalysts. a, TS-1 and modified TS-1. **b,** Magnifications of **a** in the range of 3000 to 3800 cm^{-1}.

We observed changes in the hydroxyl stretching peak of the modified TS-1 samples. Extended Data Fig. 18b reveals the emergence of a distinct band at 3689 cm^{-1} after hydrothermal modification. These spectral alterations suggest that the modification affected the framework Ti active sites, generating Ti–OH groups and eliminating the silanol nests associated with framework defects[3,4].

References

1 Li, C. *et al.* Identifying Framework Titanium in TS-1 Zeolite by UV Resonance Raman Spectroscopy. *The Journal of Physical Chemistry B* **105**, 2993-2997 (2001). https://doi.org:10.1021/jp0042359

2 Ricchiardi, G. *et al.* Vibrational Structure of Titanium Silicate Catalysts. A Spectroscopic and Theoretical Study. *J. Am. Chem. Soc.* **123**, 11409 (2001). https://doi.org/10.1021/ja010607v

3 Wu, L. *et al.* Facile synthesis of a high-performance titanosilicate catalyst with controllable defective Ti(OSi)3OH sites. *Chemical Communications* **54**, 6384-6387 (2018). https://doi.org:10.1039/C8CC02794C

4 Wang, G. *et al.* Liquid-Phase Epoxidation of Propylene with H2O2 over TS-1 Zeolite: Impurity Formation and Inhibition Study. *Industrial & Engineering Chemistry Research* **60**, 12109-12122 (2021). https://doi.org/10.1021/acs.iecr.1c02087

5 Ko, M. *et al.* Direct propylene epoxidation with oxygen using a photo-electro-heterogeneous catalytic system. *Nature Catalysis* **5**, 37-44 (2022). https://doi.org:10.1038/s41929-021-00724-9